Formation of A-type granites in the Lower Yangtze River Belt: A perspective from apatite geochemistry

Article *in* Lithos · February 2018

DOI: 10.1016/j.lithos.2018.02.005

CITATIONS
2

READS
477

7 authors, including:

Xiaoyan Jiang
Chinese Academy of Sciences
8 PUBLICATIONS **79** CITATIONS
SEE PROFILE

He Li
Chinese Academy of Sciences
29 PUBLICATIONS **557** CITATIONS
SEE PROFILE

Xing Ding
Guangzhou Institute of Geochemictry, CAS
64 PUBLICATIONS **1,253** CITATIONS
SEE PROFILE

Wu Kai
Chinese Academy of Sciences
13 PUBLICATIONS **88** CITATIONS
SEE PROFILE

Lithos 304–307 (2018) 125–134

Contents lists available at ScienceDirect

Lithos

journal homepage: www.elsevier.com/locate/lithos

Formation of A-type granites in the Lower Yangtze River Belt: A perspective from apatite geochemistry

Xiao-Yan Jiang [a], He Li [b,c,*], Xing Ding [a,d], Kai Wu [a,e], Jia Guo [a,e], Ji-Qiang Liu [f], Wei-Dong Sun [b,c,d,*]

[a] CAS Key Laboratory of Mineralogy and Metallogeny, Guangzhou Institute of Geochemistry, Chinese Academy of Sciences, Guangzhou 510640, China
[b] Laboratory for Marine Mineral Resources, Qingdao National Laboratory for Marine Science and Technology, Qingdao 266237, China
[c] Center of Deep Sea Research, Institute of Oceanology, Chinese Academy of Sciences, Qingdao 266071, China
[d] CAS Center for Excellence in Tibetan Plateau Earth Sciences, Chinese Academy of Science, Beijing 100101, China
[e] University of Chinese Academy of Sciences, Beijing 100094, China
[f] SOA Key Laboratory of Submarine Geosciences Second Institute of Oceanography State Ocean Administration, Hangzhou 310012, China

ARTICLE INFO

Article history:
Received 2 September 2017
Accepted 5 February 2018
Available online 07 February 2018

Keywords:
Apatite
Geochemical characteristics
A-type granite
Fluid metasomatism
Lower Yangtze River Belt

ABSTRACT

Apatite is ubiquitous in A-type granites, and can be used to elucidate the volatile contents of the silicate melt, which reflect its source characteristics. A-type granites have been recognized as a distinct group of granites. A_1- and A_2-type subgroups are produced under different extensional settings. However, the details of the mechanisms behind the distinctive geochemical characteristics of A_1- and A_2-type granites remain obscure. Belts of Cretaceous A_1- and A_2-type granites occur along the Lower Yangtze River Belt in eastern China. Here we investigated the major and trace element compositions of apatites from contemporary A_1- and A_2-type granites at different localities along the Lower Yangtze River Belt, in order to decipher their discrepant source processes. Apatites from A_1- and A_2-type granites show similar major and trace elements, but differ in their F and Cl concentrations. Apatites from A_1-type granites in the eastern part of the Lower Yangtze River Belt have much lower F and higher Cl concentrations compared to A_2-type granites in the western part. Moreover, from the east to the west, the F concentrations of apatites from A_1-type granites increase, while the Cl concentrations decline. In a subducted plate, F is retained by amphibole, chlorite, serpentine and mica minerals through the amphibolite stage, and finally by phengite and lawsonite during the eclogite stage, whereas, Cl is controlled by amphibole, chlorite and serpentine. The high and varied Cl concentrations in A_1 subgroup apatites, therefore, may be attributed to the breakdown of amphibole, chlorite and/or serpentine decomposition during partial melting of subducted oceanic crust releasing a large amount of Cl at shallower depth. In contrast, F is transported to deeper depths in the subducted oceanic crust, and released through breakdown of phengite and lawsonite, making an important contribution to the formation of A_2-type granites. Apatites from A_1- and A_2-type granite samples show regular changes in LREE/HREE, LREE/MREE and MREE/HREE ratios with increasing distance from the location of the subduction zone, probably as the result of nonsynchronous dehydration of the serpentine and phengite at different stages during subduction. We propose that A_1- and A_2-type granites on the Lower Yangtze River Belt were derived from sources metasomatised by fluids originating from the breakdown of amphibole, chlorite and/or serpentine with higher Cl, lower F, and from phengite and/or lawsonite with relatively higher F but lower Cl, respectively.

1. Introduction

Magmatic volatiles (i.e., F, Cl, S, C and H_2O) play an important role in defining magmatic physicochemical conditions and evolutionary processes (e.g., Harlov, 2015; Webster and Piccoli, 2015). Apatite is a prime mineral for understanding volatile compositions because it can accommodate a number of these volatiles directly into its crystal structure (Harlov, 2015). Furthermore, apatite contains elements sensitive to high-temperature magma evolution (LREE-MREE, Mn), is ubiquitous in virtually all geochemical systems, and is stable over a wide range of P-T fields (Konzett and Frost, 2009). Thus, apatite is a superb mineral to elucidate the volatile contents of the magmas, to provide further information on metasomatic process (Boyce and Hervig, 2009; Harlov, 2015; Piccoli and Candela, 1994) and to trace petrogenetic processes, which are not always obvious using whole-rock methods (Bruand et al., 2017; Miles et al., 2014; Parat et al., 2011).

A-type granite is a special type of granitoid that is believed to originate from anhydrous but halogen-rich (especially F) magmas (Bonin,

* Corresponding authors at: Laboratory for Marine Mineral Resources, Qingdao National Laboratory for Marine Science and Technology, Qingdao 266237, China.
E-mail addresses: lihe@qdio.ac.cn (H. Li), weidongsun@qdio.ac.cn (W.-D. Sun).

https://doi.org/10.1016/j.lithos.2018.02.005
0024-4937/

2007; Collins et al., 1982; Clemens et al., 1986; Eby, 1990; Loiselle and Wones, 1979; Whalen et al., 1987). The nature of the processes and mechanisms responsible for A-type granite formation is one of the most debated topics in igneous petrology (Bonin, 2007). Various models and classification schemes have been proposed to describe and explain their petrogenesis and geological significance (Clemens et al., 1986; Collins et al., 1982; Creaser et al., 1991; Eby, 1992; Frost and Frost, 2011; Huang et al., 2011; Loiselle and Wones, 1979; Patiño Douce, 1997; Whalen et al., 1987; Yang et al., 2006). The earliest and most common classification scheme divides A-type granites into A_1 and A_2 subgroups (Eby, 1992). A_1-type granites generally occur in the intraplate environment with chemical compositions similar to oceanic-island basalts, whereas, A_2-type granites usually occur in post-collisional settings with chemical characteristics similar to island-arc basalts (Eby, 1992). The genesis of A_1 and A_2 subgroups has also been proposed to involve varying degrees of subduction-induced mantle metasomatism (Li et al., 2012a). Thus, the details surrounding the mechanism controlling the formation of A-type granites still remains controversial.

Large amounts of Cretaceous A-type granites are distributed along the Lower Yangtze River Belt (LYRB) in eastern China. Interestingly, both A_1 and A_2 subgroups were emplaced during the same period ~125 Ma (e.g., Li et al., 2012a; Xing and Xu, 1994). Previous studies have interpreted them as being products of extension in a postorogenic setting (e.g., Su et al., 2013; Xing and Xu, 1994), or slab-roll back (e.g., Yang et al., 2016), or extension after ridge subduction (Li et al., 2011, 2012a; Ling et al., 2009). However, the particular mechanism behind how different A-type subgroups formed during the same geological event needs to be better constrained. In this study, the chemistry of apatites from five A-type granitic plutons, distributed across the subduction zone in the LYRB, have been studied in order to shed new light on the contribution of fluid metasomatism to the source materials responsible for the formation of A-type granites.

2. Geological background

The LYRB is located on the northeastern margin of the Yangtze Block (Fig. 1), adjacent to the Dabie-Sulu orogenic belt, and is bordered by the Xiangfan-Guangji and Tancheng-Lujiang faults in the northwest, and separated from the Cathaysia Block by the Jiangshan-Shaoxing fault in the south (Fig. 1c). The main outcrops in the region are composed of a low-grade Neoproterozoic clastic metasedimentary series with minor volcanic rocks and Paleozoic-Triassic sedimentary strata, which subsequently were intruded by Late Mesozoic magmatic rocks (150 to 110 Ma) (Fig. 1c; Song et al., 2014; Yang and Zhang, 2012). A-type granites mainly developed between 129 and 120 Ma, and define two parallel magmatic belts within the Dalongshan- Zongyang- Huangmeijan belt in the north and the Huayuagong- Maotan- Baishiling- Xianshuijian belt in the south (Li et al., 2011, 2012a; Ling et al., 2009; Su et al., 2013; Wong et al., 2009; Xing and Xu, 1994; Yang et al., 2016; Zhang et al., 1988).

We have analyzed apatite compositions in six samples from five previously studied A-type plutons in the LYRB. They are, from east to west, Xiangshuijian (XSJ), Banshiling (BSL), Maotan (MT), Huayuangong

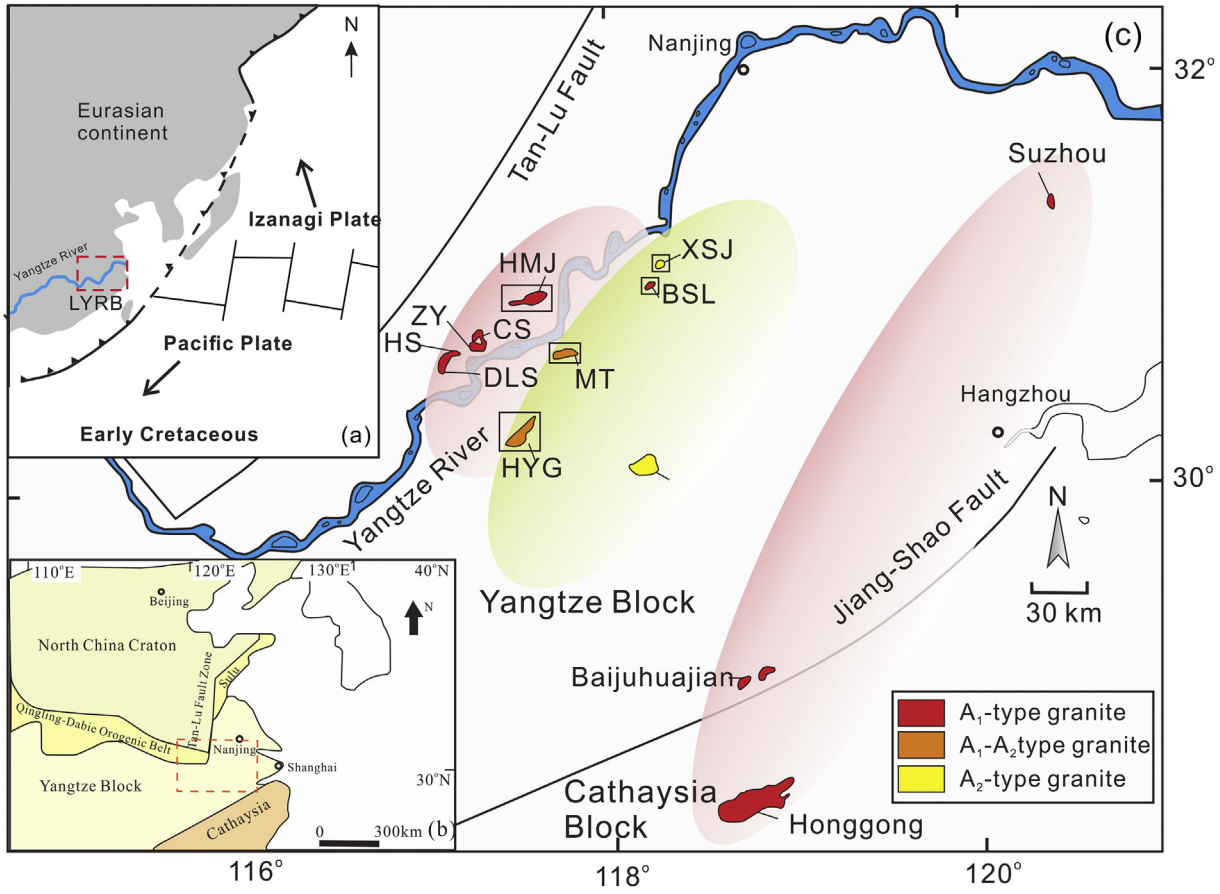

Fig. 1. Geological map of the Lower Yangtze River Belt (LYRB). (a) Ridge subduction between the Izanagi and Pacific plates of eastern China in the LYRB during Early Cretaceous. The black arrows show the direction of plate drift: Izanagi plate was moving north-northwestward and Pacific plate southwestward. The paleo-subduction zone is presumed to be situated at the coastline (modified after Maruyama et al., 1997; Sun et al., 2007b; Ling et al., 2009) (b) Tectonic sketch map of eastern China (after Su et al., 2013); (c) distribution of A-type granitoids in the LYRB (after Li et al., 2012a, 2012b; Yang et al., 2016), DLS (Dalongshan), HS (Huashan), ZY (Zongyang), CS (Chengshan), HMJ (Huangmeijian) granites on the north bank of the LYRB (compiled from Fan et al. (2008) and Li et al. (2011)) and BSL (Banshiling) on the south bank of the LYR are A_1-type granites; HYG (Huayuangong) and MT (Maotan) granites on the south bank of the LYRB have both A_1 and A_2 chemical group granites. Huangshan granite (compiled from Xue et al. (2009) and Zhang et al. (2009)) and XSJ (Xiangshuijian) granites are A_2-type granites.

(HYG) and Huangmeijian (HMJ) plutons, which are located at an increasing distance to the proposed paleo-subduction belt parallel to the coastline (Sun et al., 2007b; Ling et al., 2009). The A-type granites crop out in roughly parallel zones, with A_1- and A_2-type granites alternately distributed (Li et al., 2012a; Fig. 1c). Details of each pluton are as follows.

The XSJ A_2-type granite (31°02.23 N, 118°13.70 E) nearest to the paleo-subduction zone, is an alkali-feldspar granite located at the southeastern part of the Fanchang Basin (Fig. 1c). It consists of quartz (22–28 vol%), K-feldspar (64–67 vol%), plagioclase (2–3 vol%), and biotite (5–8 vol%) (Li et al., 2012a; Xing and Xu, 1994).

The BSL A_1-type granite (31°07.38 N, 118°17.65 E) located close to the XSJ pluton, crops out in the southeastern Fanchang Basin, and covers an area of about 16 km^2 (Fig. 1c; Lou and Du, 2006). It is a quartz monzonite, containing quartz (12–14 vol%), K-feldspar (43–48 vol%), plagioclase (30–40 vol%), and biotite (5–8 vol%) (Li et al., 2012a).

The MT and HYG pluton are both situated at the transitional part of the proposed A_1- and A_2-type granite zones (Li et al., 2012a), and occur at similar distances to the subduction belt. The MT granite (30°41.70 N, 117°47.28 E) is situated in the Anqing-Guichi area, and crops out over about 25 km^2 (Wu and Zhou, 1998). The granite consists of an alkaline feldspar granite and quartz syenite with granitic, porphyritic, and graphic textures. It consists of quartz (7–22 vol%), K-feldspar (76–79 vol%), plagioclase (1–4 vol%), and biotite (0.5–3 vol%) (Li et al., 2012a; Xing and Xu, 1994). The HYG granite (30°37.58 N, 117°36.33 E) is located in Anqing-Guichi area (Fig. 1c). The granite is a medium- to fine-grained alkali feldspar granite with a miarolitic texture, and is composed of quartz (25–33 vol%), K-feldspar (64–67 vol%), plagioclase (2.5–3 vol%), and biotite (<1 vol%) (Li et al., 2012a).

The westernmost HMJ A_1-type granite (30°56.26 N,117° 35.14 E) located in Luzong Basin and most far away from the inferred paleo-subduciton zone, is a faint red moderate- to coarse-grained alkaline granite (Li et al., 2011). It consists of K-feldspar (80–85 vol%), quartz (10–15 vol%), and plagioclase (5–10 vol%) (Li et al., 2011; Zheng et al., 1995).

3. Analytical methods

Apatite crystals were separated from the A-type granites and then cast in epoxy. The mount was then polished to expose a cross section of the apatite grains for electron microprobe (EMP) and laser ablation inductively coupled-plasma mass spectrometry (LA-ICP-MS) analyses.

Major elements in the apatite were analyzed using a JXA-8100 electron microprobe operated with wavelength-dispersive spectrometers (WDS) at the State Key Laboratory of Mineral Deposits Research, Nanjing University, Nanjing, China (Table 1 and Table A.1). The analyses were conducted using a 15 keV, 10 nA, 10 μm defocused electron beam. The standards used were norbergite for F, $Ba_5(PO_4)_3Cl$ for Cl, and apatite for Ca and P analyses. Fluorine and Cl were analyzed for 10 s in order to avoid volatile loss. Count times for other elements were 20 s. Fluorine and Cl were measured using the Kα line on a LDE1 crystal and a PET crystal, respectively (Li et al., 2012b). Analytical precision for most of the major elements is better than 1%, but for F and Cl precision is around 5%.

Minor and trace element abundances in apatite were determined using a LA-ICP-MS at the Key Laboratory of Mineralogy and Metallogeny, Guangzhou Institute of Geochemistry, Chinese Academy of Sciences (GIG-CAS). The Agilent 7500a ICP-MS instrument is coupled to a Resonetics 193 nm ArF excimer laser ablation system. In situ LA-ICP-MS analyses of apatite were performed on the same spot where EMP analyses were conducted. The operating conditions included a 80 mJ laser energy, ablation frequency of 8 Hz, and a laser beam spot size of 43 μm. Helium was used as the carrier gas. The Ca concentration, obtained by EMP analysis, was used as the internal standard. The NIST SRM 610 was analyzed as an external standard. The NIST SRM 612 standard was employed as a reference (Li et al., 2014). Data reduction was performed using the ICPMSDataCal software (after Lin et al., 2016; Liu et al., 2008). Apatite minor and trace element concentrations are listed in Table 1 and Table A.1. The LA-ICP-MS detection limit is <0.1 ppm and the analytical uncertainty is better than 10% (relative percentage) for most of the elements analyzed.

The whole-rock major and trace elements of these representative samples have been analyzed by Li et al. (2011, 2012a), and are shown in Table A.2.

4. Results

All apatites are of fluorapatite composition and mostly intact prismatic crystals with smooth surface planes, which are typical for igneous apatite (Nash, 1984). While being predominantly fluorapatite in composition, halogen concentrations for apatites from the various A-type granite samples are variable in the LYRB. Fluorine concentrations range from 1.47 to 2.97 wt%, and Cl concentrations vary from 0.01 to 1.47 wt% (Table 1 and Table A.1; Fig. 2), while F/Cl ratios range from 1.0 to 438. The mole percent of OH can be estimated by the structural formula, and varies from 0.44 to 0.19 wt%. Apatites from the A_1 subgroup plutons have varied F and Cl contents, ranging from 1.47 to 2.97 wt%, and from 0.02 to 1.47 wt%, respectively, and these contents are negatively correlated. However, apatites from the A_2 subgroup have relatively high F and low Cl concentrations, varying from 2.07 to 2.69 wt% for F, and from 0.01 to 0.14 wt% for Cl. Apatites from the BSL pluton (A_1 subgroup) show the lowest F/Cl ratios (below 2) and the highest Cl concentrations (from 0.23 to 1.47 wt%). In contrast, apatites from the HYG pluton (A_2 subgroup) have the highest F/Cl ratios (up to 218) and the lowest Cl concentrations (below 0.05 wt%).

Apatites from the two granite subgroups have similar MnO, FeO, and MgO contents. Most of the apatites contain high MnO contents from ≈0.1 wt% up to 0.8 wt% and FeO up to 0.2 wt%, but with low MgO (<0.09 wt%; Table 1 and Table A.1).

Vanadium can enter apatite in the form of VO_4^{3-} where it directly substitutes for PO_4^{3-} (Kutoglu, 1974; Wilson et al., 1977). Variable V contents (0.12 to 38.7 ppm; Table 1 and Table A.1) are observed in the apatites. V contents in apatites from the A_2 subgroup are relatively higher (3.75 to 38.7 ppm) compared to those from the A1 subgroup (0.12 to 38.2 ppm) (Table 1 and Table A.1). The higher V abundances in the A2 granites cannot be attributed to the degree of oxidation, but rather the high V concentrations appear to be related to V abundances in the source rocks of the granites (Table A.2). Apatites from A-type granites have varied Sr concentrations (from 18.7 to 628 ppm; Table 1 and Table A.1) and Y concentrations (from 717 to several thousand ppm; Table 1 and Table A.1), and an especially large range in Y contents for the apatites from the HMJ (1654–9611 ppm). The varied and low Sr and Y concentrations may suggest that plagioclase and garnet co-crystallized with apatite in during formation of the A-type granites.

Apatites from the A-type granite subgroups show similar chondrite-normalized REE patterns (Fig. 3). The apatites are all marked by a slightly inclined REE pattern (LREE-enriched) with high $(La/Yb)_N$ ratios and negative Eu-anomalies (Fig. 3). Apatites from BSL01 exhibit the lowest $(La/Yb)_N$ ratios (mean value of 12.0; Fig. 4), while apatites from XSJ09 display the highest $(La/Yb)_N$ ratios (mean value of 21.8; Fig. 4). Apatites display strong negative Eu-anomalies (Eu/Eu^* of 0.17 to 0.02), among which sample HMJ02 has the strongest Eu depletions (0.05 to 0.02). Cerium concentrations in the apatites are all higher than 3000 ppm, and attain tens of thousands of ppm in sample HMJ02.

5. Discussion

5.1. Volatile contents of melt

Fluorine and Cl play an important role during magmatic evolution by depolymerizing the melt structure and, in particular, enabling hydrothermal metal transport and ore deposition during degassing and fluid exsolution (e.g., Dingwell et al., 1998; Filiberto and Treiman, 2009;

Table 1
Representative major, minor and trace element apatite compositions from the Early Cretaceous A-type granites of the LYRB.

Sample No.	P_2O_5	SiO_2	CaO	SrO	MnO	MgO	FeO	F	Cl	Sum	F═O	Cl═O	Total	OH	V	Y	La	Ce	Pr	Nd	Sm	Eu	Gd	Tb	Dy	Ho	Er	Tm	Yb	Lu	Sr
	wt%	wt%	wt%	wt%	wt%	wt%	wt%	wt%	wt%	wt%	wt%	wt%	wt%	Mole fraction	ppm	ppm	ppm	ppm	ppm	ppm	ppm	ppm	ppm	ppm	ppm	ppm	ppm	ppm	ppm	ppm	ppm
BSL9-01	41.53	0.31	52.33	0.01	0.75	0.09	0.23	1.51	1.45	97.2	0.63	0.33	96.3	0.38	14.1	1912	1813	4555	566	2349	472	24.8	401	56.1	326	65.8	174	24.4	152	21.3	202
BSL9-02	41.57	0.31	53.86	–	0.37	0.05	0.10	1.70	1.21	98.2	0.71	0.28	97.2	0.37	13.6	2206	1837	5067	643	2714	561	26.7	472	66.8	386	76.4	203	28.0	177	24.1	163
BSL9-03	41.88	0.40	53.36	0.01	0.20	0.04	0.08	1.57	1.26	97.8	0.66	0.29	96.9	0.39	19.5	1581	3250	6968	786	3100	535	37.3	418	53.9	300	58.2	155	21.4	135	18.0	326
BSL9-04	40.76	0.34	54.14	–	0.23	0.05	0.08	1.76	1.21	97.6	0.74	0.28	96.5	0.35	23.9	1149	2520	5419	621	2555	444	47.3	355	43.3	231	44.1	105	13.1	74.4	10.2	400
BSL9-05	42.23	0.26	53.33	0.01	0.37	0.01	0.17	1.75	0.95	98.1	0.73	0.22	97.2	0.39	10.2	2175	1477	4253	560	2398	526	32.0	455	65.6	380	76.1	204	29.5	195	26.7	238
HMJ2-03	42.11	0.50	53.42	–	0.20	–	0.06	2.31	0.04	97.7	0.97	0.01	96.7	0.37	6.57	1763	4829	10,661	1265	5119	870	16.8	636	73.6	361	61.2	140	16.9	93.0	11.6	54.9
HMJ2-05	39.83	1.69	51.67	0.02	0.12	0.00	0.11	2.20	0.04	94.7	0.93	0.01	93.8	0.38	0.53	7175	4282	11,693	1582	7182	1768	28.1	1593	233	1329	254	652	91.4	538	62.2	130
HMJ2-06	41.77	0.73	53.73	0.01	0.17	0.05	0.14	2.97	0.04	98.3	1.25	0.01	97.1	0.19	6.50	1648	3725	8320	1022	4215	757	33.0	589	67.5	337	58.6	134	16.6	94.1	12.2	152
HMJ2-07	41.48	0.48	53.59	0.01	0.17	0.01	0.11	2.39	0.04	97.3	1.00	0.01	96.3	0.35	5.98	1746	4526	10,322	1239	5197	908	27.1	711	77.3	377	66.0	145	17.5	93.4	12.4	55.1
HMJ2-08	41.34	0.62	54.04	0.01	0.07	–	–	2.20	0.03	97.4	0.92	0.01	96.4	0.40	0.12	3417	3009	7582	933	3871	840	12.8	760	106	599	115	292	39.3	230	30.6	198
HYG3-01	42.88	0.09	54.35	–	0.13	0.06	0.14	1.86	0.95	99.5	0.78	0.22	98.5	0.37	28.6	920	2298	4890	551	2213	376	19.2	276	33.9	180	32.7	81.0	10.4	62.2	8.10	260
HYG3-02	42.54	0.44	53.76	0.02	0.41	0.02	0.04	2.55	0.03	98.7	1.07	0.01	97.6	0.31	24.7	849	2575	4411	366	1133	146	12.3	127	16.9	108	23.8	73.9	11.3	77.2	11.7	102
HYG3-03	41.19	0.93	53.62	0.01	0.49	0.00	0.05	2.63	0.02	97.8	1.11	0.00	96.7	0.29	8.09	2653	4181	8978	951	3536	592	32.9	527	74.6	448	91.1	246	32.2	194	25.5	18.7
HYG3-04	43.33	0.12	54.16	0.01	0.06	0.08	0.13	2.06	1.02	99.9	0.86	0.23	98.8	0.31	22.5	717	2262	4688	515	2050	339	16.9	245	28.9	150	26.6	64.1	8.09	48.7	6.18	213
HYG3-06	41.81	0.64	54.13	0.00	0.29	0.02	0.11	2.43	0.02	98.4	1.02	0.00	97.4	0.35	3.71	2374	4045	8177	740	2373	349	15.0	317	48.5	325	72.6	212	29.8	187	25.0	40.1
XSJ9-01	41.89	0.36	54.40	0.01	0.45	0.02	–	2.51	0.10	98.6	1.05	0.02	97.6	0.31	17.4	1623	3856	7427	722	2560	377	16.1	325	41.7	238	51.4	149	19.3	126	18.9	237
XSJ9-02	41.46	0.46	53.93	0.01	0.41	0.02	0.03	2.28	0.09	97.7	0.96	0.02	96.7	0.37	20.6	1791	3722	7357	728	2670	406	17.0	344	44.6	261	56.2	160	21.3	133	19.5	291
XSJ9-03	41.64	0.28	53.93	0.01	0.30	0.02	0.09	2.10	0.11	97.6	0.88	0.03	96.7	0.42	38.7	1043	2787	5567	585	2384	371	18.2	276	32.1	169	33.7	92.4	12.2	79.6	12.0	204
XSJ9-04	41.35	0.39	53.85	–	0.46	0.01	0.02	2.22	0.09	97.4	0.93	0.02	96.5	0.39	21.8	1180	2798	5950	670	2794	450	35.9	331	40.5	209	40.5	103	13.2	79.5	11.2	107
XSJ9-05	42.23	0.25	54.53	0.03	0.31	0.02	0.04	2.08	0.05	98.7	0.87	0.01	97.8	0.44	26.1	1250	2723	5173	506	1859	311	11.2	288	36.3	199	41.9	114	14.4	85.6	12.8	159
MT12-01	42.62	0.31	54.25	–	0.15	0.04	0.11	2.48	0.05	99.0	1.04	0.01	97.9	0.33	27.7	1327	2305	5165	621	2542	468	51.5	378	49.6	269	49.1	124	15.3	82.5	10.9	174
MT12-02	42.25	0.53	54.23	–	0.17	0.06	0.16	2.39	0.08	98.8	1.00	0.02	97.8	0.35	15.6	1977	3009	6915	852	3563	667	89.1	552	72.4	401	75.1	183	23.0	128	17.1	457
MT12-03	42.74	0.24	54.32	0.03	0.23	0.04	0.15	2.42	0.07	99.2	1.02	0.02	98.2	0.34	30.9	1350	2293	5211	623	2578	475	48.0	385	49.5	271	51.1	123	14.7	82.1	10.7	168
MT12-04	42.48	0.30	54.00	0.02	0.17	0.05	0.05	2.48	0.07	98.6	1.04	0.02	97.5	0.33	22.8	1339	2288	5110	612	2525	470	53.6	378	49.3	264	50.2	122	15.2	81.4	10.9	243
MT12-06	42.76	0.41	54.66	0.03	0.07	0.03	0.10	2.40	0.06	99.5	1.01	0.01	98.5	0.36	15.6	1350	2754	5497	606	2464	447	52.9	371	48.2	262	50.8	123	16.2	89.6	12.6	251
HYG1-01	42.50	0.60	54.22	0.01	0.29	0.01	0.10	2.38	0.03	99.1	1.00	0.01	98.1	0.36	6.89	1876	4349	7738	658	1999	263	18.6	223	33.0	222	52.6	165	25.1	172	24.5	53.3
HYG1-02	41.82	0.39	53.85	0.01	0.26	0.02	0.04	2.50	0.01	97.8	1.05	0.00	96.8	0.32	6.70	1314	4378	7706	638	1936	240	19.7	189	25.6	158	37.2	113	17.7	122	18.0	86.7
HYG1-03	42.04	0.27	54.14	–	0.25	0.04	0.02	2.61	0.01	98.3	1.10	0.00	97.2	0.30	23.7	847	2608	4654	421	1447	204	16.7	172	21.6	124	26.8	74.9	10.7	69.3	10.2	99.8
HYG1-04	41.80	0.77	53.61	0.01	0.36	0.02	0.09	2.36	0.05	98.1	0.99	0.01	97.1	0.36	3.75	3300	4856	9789	962	3241	545	22.1	552	84.4	529	115	306	39.5	236	31.5	67.8
HYG1-05	42.19	0.43	54.06	–	0.29	0.02	0.05	2.62	0.02	98.6	1.10	0.00	97.5	0.30	8.26	2032	4166	7692	685	2096	285	17.5	258	38.2	252	61.1	185	27.2	176	25.4	48.3

Harlov, 2015). However, tracing their evolution in magmatic systems is not an easy task. Whole-rock F and Cl concentrations may not directly reflect primary F and Cl abundances in the melt, but these can be traced by F- and Cl-rich minerals, such as apatite (e.g., Bonin, 1988; Zhang et al., 2012). Apatite provides a strong diagnostic capability for the geochemical behavior of lithophile elements in magmatic fluids (Hughes and Rakovan, 2015), but the presence of F and Cl allows apatite to act as a monitor of the behavior of volatile components in magmas as well (Webster et al., 2009). The abundances of F and Cl in melts can be estimated from the F and Cl concentrations in apatite using available mineral/melt partitioning models (Doherty et al., 2014; Mathez and Webster, 2005; Prowatke and Klemme, 2006; Webster et al., 2009). Moreover, the mass balance calculation for Cl in melt-mineral systems indicates that the crystallization of apatite cannot lead to a strong enrichment or depletion of Cl in granitic melts, which might explain the near constant Cl concentration over a large temperature range. Similarly, F concentrations derived from apatite compositions do not change significantly within the crystallization interval (Zhang et al., 2012). Thus, the F and Cl contents estimated from apatite/melt partitioning can be regarded as primary indicators of the composition of the granitic magma.

In the LYRB, the F and Cl concentrations of apatites from the A_1 granite subgroup show a negatively correlated relationship, with those in the BSL A_1-type granite subgroup near to the subduction zone having the lowest F and the highest Cl concentrations (Figs. 1c and 2). Apatites from other A_1-type granites, further away from the subduction zone, have relatively higher and varied F and lower Cl concentrations (Figs. 1c and 2). In comparison, all A_2-type granites in this study have apatites with high F and low Cl concentrations (Fig. 2).

Here, utilizing the apatite compositions, published apatite-melt partition coefficients are used to estimate the volatile concentrations in the melt prior to ascent and degassing. Several experimental and theoretical studies have been addressed to investigate the partitioning of F and Cl in apatite-melt-fluid systems (e.g., Doherty et al., 2014; Mathez and Webster, 2005; Prowatke and Klemme, 2006; Webster et al., 2009). Among these, Webster et al. (2009) determined the partitioning of F and Cl between rhyolitic to rhyodacitic melts and apatite at ca. 200 MPa and 924–900 °C, which are close to the conditions of magmatic emplacement for A-type granites in the LYRB (Table A.2). Here, several experiments were run to determine the partition coefficients under a specific redox state (Webster et al., 2009). When the system is buffered to Ni-NiO oxygen fugacity, $D_F^{apat/melt} = 12.7$ and $D_{Cl}^{apat/melt} = 3.5$ (Webster et al., 2009), which are most appropriate $\log f_{O2}$ conditions for estimating the volatile compositions of A-type granites in the LYRB (Fig. 5; Table A.3). The calculated F and Cl concentrations of the granitic melts range from 1160 to 2341 ppm and 14 to 4191 ppm (Fig. 6), respectively. The difference between the A_1- and A_2-type granites is that the Cl concentrations of A_1 granitic melt are mostly higher than 1000 ppm, with a small subset lower than 300 ppm. This is in contrast to the lower Cl concentrations in the A_2-type granitic melt (<300 ppm) (Fig. 6). It has been proposed that the differences in F and Cl concentrations might be due to the source materials or late-stage magmatic process (Collins et al., 1982). Considering where each of the two granite types were sampled in the LYRB, the composition of the melt source may exert a stronger influence on the volatile components of the derived melts. However, F and Cl abundances in the primitive mantle are estimated at 25 and 17 ppm, respectively (e.g., McDonough and Sun, 1995), and an order of magnitude higher in the average continental crust (553 and 244 ppm, respectively, Rudnick and Gao, 2003). Thus, there must be other geological processes responsible for fertilizing the source areas with volatile components. Combined with the previous study (Li et al., 2012a), mantle metasomatism may play a critical role in determining the F- and/or Cl-riched magma sources of the A-type granites in the LYRB.

5.2. Discrepant mantle metasomatic processes in the LYRB

Metasomatism of the mantle wedge has been recognized as a widespread process during subduction, because it is associated with continuous release of fluid through the overriding mantle from downgoing subducting slabs. Fluorine and Cl are volatile trace elements that can be incorporated into some hydrous minerals and variously released during geological processes. In general, F is mainly retained by phengite and lawsonite during plate subduction, and released at deep depths (Fig. 7). In contrast, Cl is held by amphibole, chlorite and serpentine, expelled earlier during plate subduction (e.g., Debret et al., 2013, 2014; Deschamps et al., 2013; Pagé et al., 2016; Scambelluri et al., 2004; Schmidt et al., 2004; Sun et al., 2007a; Xiong et al., 2005, 2009; Fig. 6). In addition, serpentine and phengite are both contributors of REEs to the mantle wedge, and will release varying amounts of REEs in different

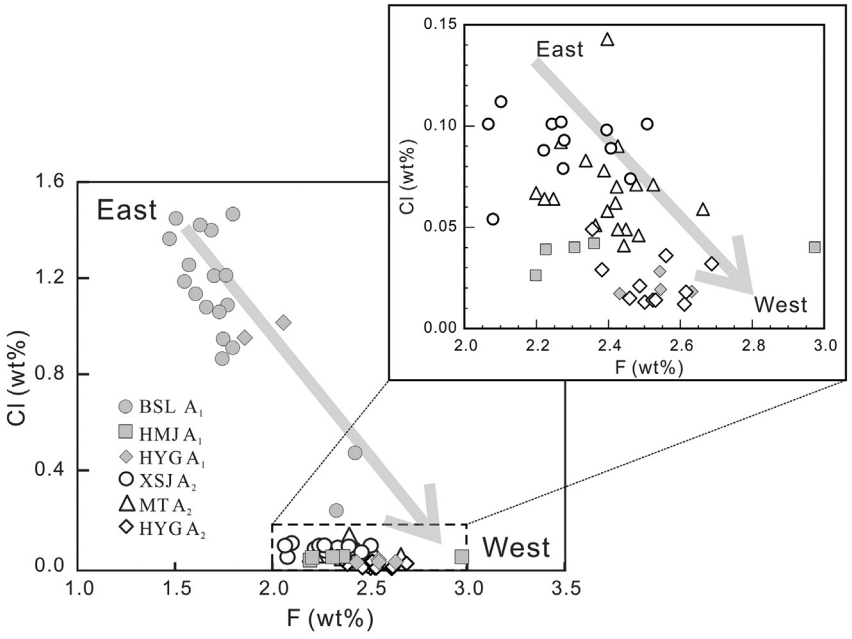

Fig. 2. Apatite-F versus apatite-Cl from the A-type granites in the LYRB.

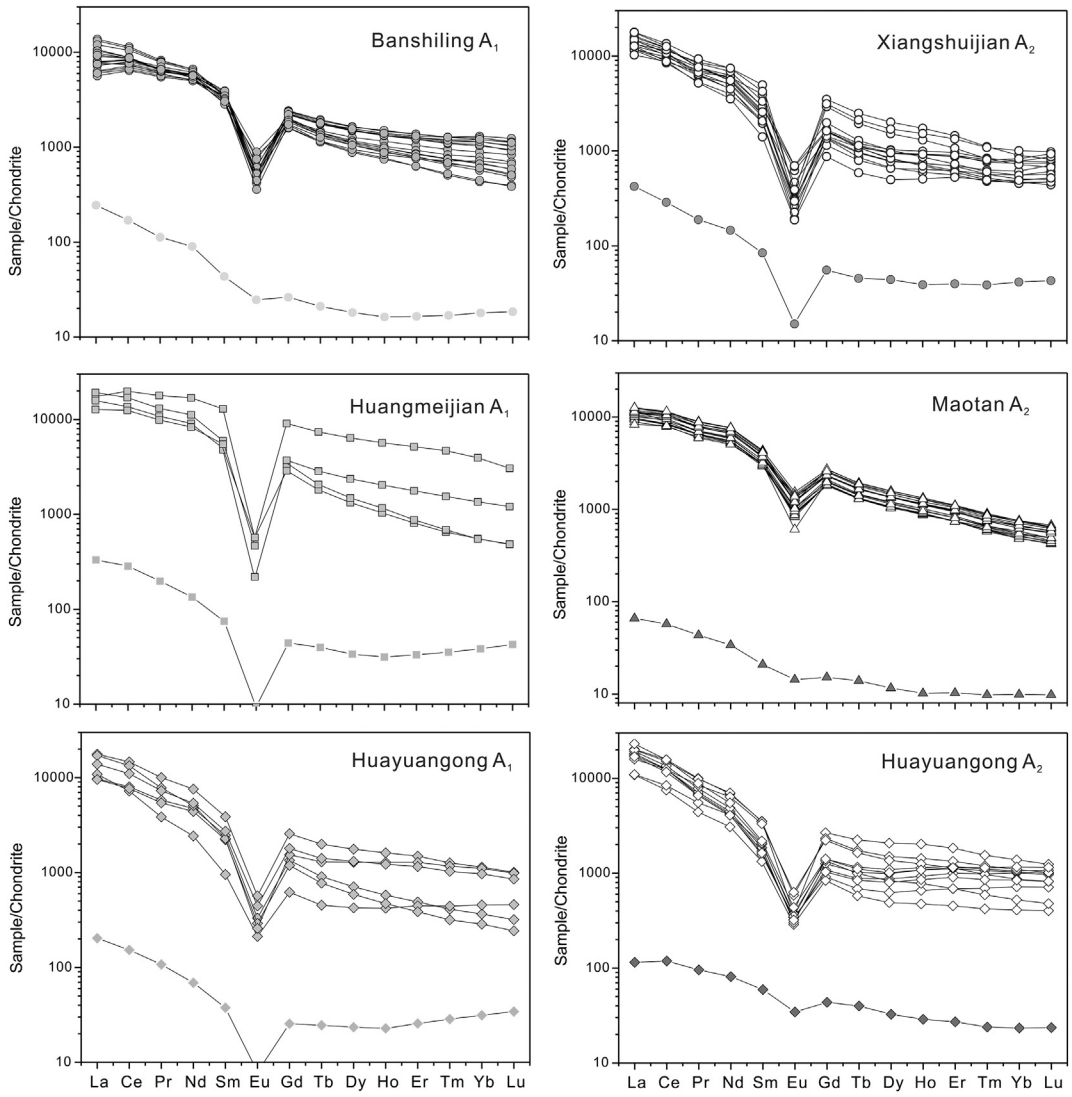

Fig. 3. Chondrite-normalized REE patterns of apatites (upper part of the diagram) and their host-rocks (single one in the lower part of the diagram) from the LYRB. Chondrite REE abundances are from Sun and McDonough (1989).

stages of slab dehydration (Debret et al., 2013; Scambelluri et al., 2004; Schmidt and Poli, 2014).

In the LYRB, the F and Cl concentrations and REE ratios of apatites from A-type granites change regularly (Figs. 2 and 4) depending on proximity to the inferred subduction zone, from near the subduction zone (East) to further away (West) (Fig. 1a). As the subducting slab goes deeper, a lower amount of Cl is being contributed by amphibole and chlorite breakdown (Debret et al., 2014; Pagé et al., 2016; Sun

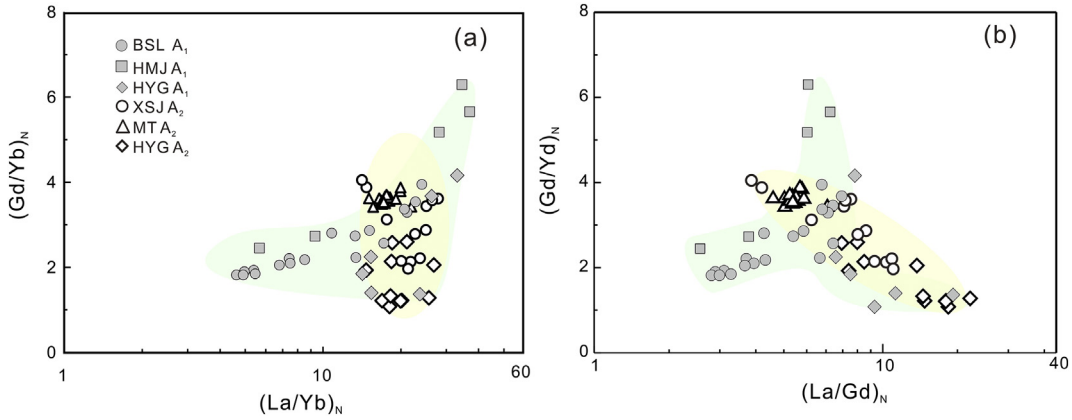

Fig. 4. (a) $(Gd/Yb)_N$ versus $(La/Yd)_N$, (b) $(Gd/Yb)_N$ versus $(La/Gd)_N$ diagrams of apatite from A-type granites in the LYRB. The green field designates the A_1-type granite and yellow for the A_2-type granite. (For interpretation of the references to color in this figure legend, the reader is referred to the web version of this article.)

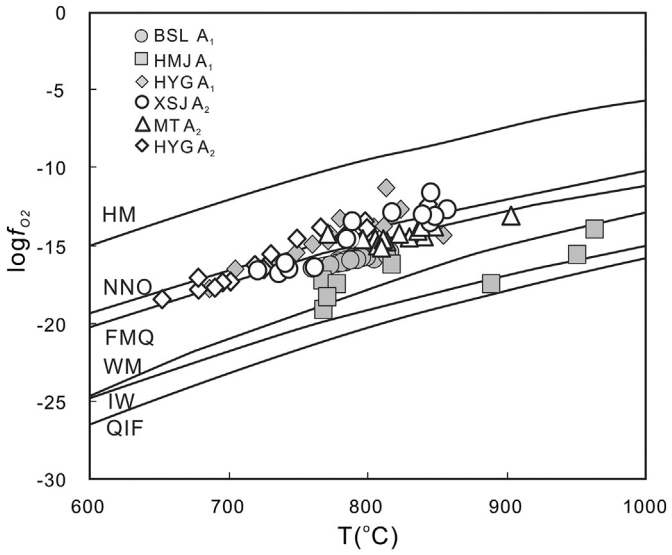

Fig. 5. Plot of $\log f_{O2}$ versus T (°C) showing oxygen fugacities of granites in the LYRB. The trace element data of zircons are from Li et al. (2011, 2012a, 2012b). Values of $\log f_{O2}$ calculated using the Ce-in-zircon oxygen barometer (Smythe and Brenan, 2016) as a function of the Ti-in-zircon temperature (Watson and Harrison, 2005). MH = magnetite-hematite buffer; NNO = nickel-nickel oxide buffer; FMQ = fayalite-magnetite-quartz buffer; IW = iron-wustite buffer; QIF = quartz-iron-fayalite buffer. Buffer curves from Frost and Lindsley (1991).

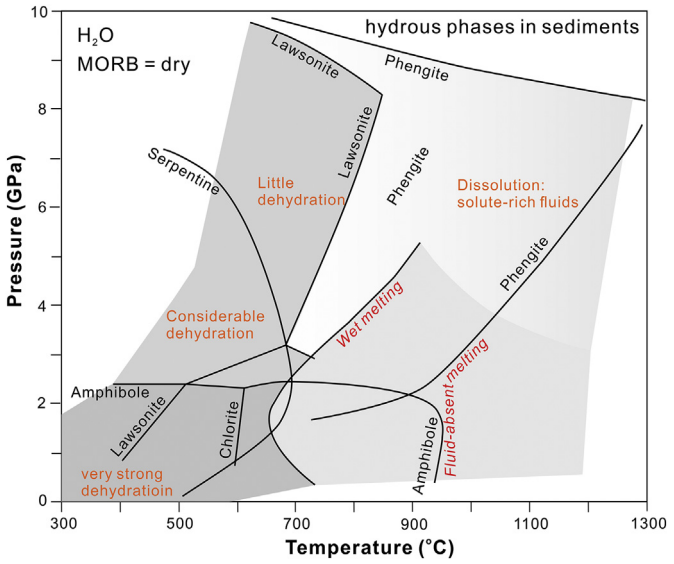

Fig. 7. Pressure-Temperature diagram shows the P-T stability fields for amphibole, chlorite, serpentine, phengite and lawsonite. Devolatilization regimes during subduction are mainly based on phase relations in MORB (Schmidt and Poli, 2014). H_2O-saturated melting takes place in MORB and sediments at the wet solidus; fluid-absent melting to 2.5 GPa is dominated by amphibole (MORB) or biotite (pelite) and above 2.5 GPa by phengite (only in pelites).

et al., 2007a; Figs. 7 and 8). Serpentine is another contributor of Cl to the mantle wedge (Debret et al., 2013, 2014; Scambelluri et al., 2004). At shallow depths ($T < 300$ °C), chrysotile alters to antigorite releasing 90% of the Cl (Kodolányi and Pettke, 2011). That is, away from the subduction zone the overlying mantle wedge above the subducted slab was metasomatized by fluids with decreasing Cl contents (Fig. 8), during the formation of A_1-type granite. This could plausibly explain the Cl concentrations of the BSL A_1-type granite (near the subduction zone), and being much higher than the HMJ A_1-type granite (far away from the subduction zone) (Figs. 2 and 6). In contrast, F is controlled by the phengite and lawsonite, decomposing at greater depth under higher pressure (Pagé et al., 2016; Schmidt et al., 2004; Figs. 7 and 8). Further away from the subduction zone at deep levels, the breakdown of phengite and lawsonite will produce a fluid enriched in F, metasomatising the mantle wedge (Churikova et al., 2007; Pagé et al., 2016; Schmidt and Poli, 2014), and making contributions to the generation of A_2-type granite. Partial melting of such a source leads to XSJ, MT and HYG A_2-type granites that have high F and low Cl concentrations (Fig. 2).

Serpentine and phengite are both contributors of REEs to the mantle wedge. Through increasing grade, chrysotile transforms to antigorite, and more LREE are released than MREE and HREE (Debret et al., 2013), resulting in the metasomatized mantle source for A_1-type granites (BSL and HMJ) that is enriched in LREE (Figs. 3 and 4). With further

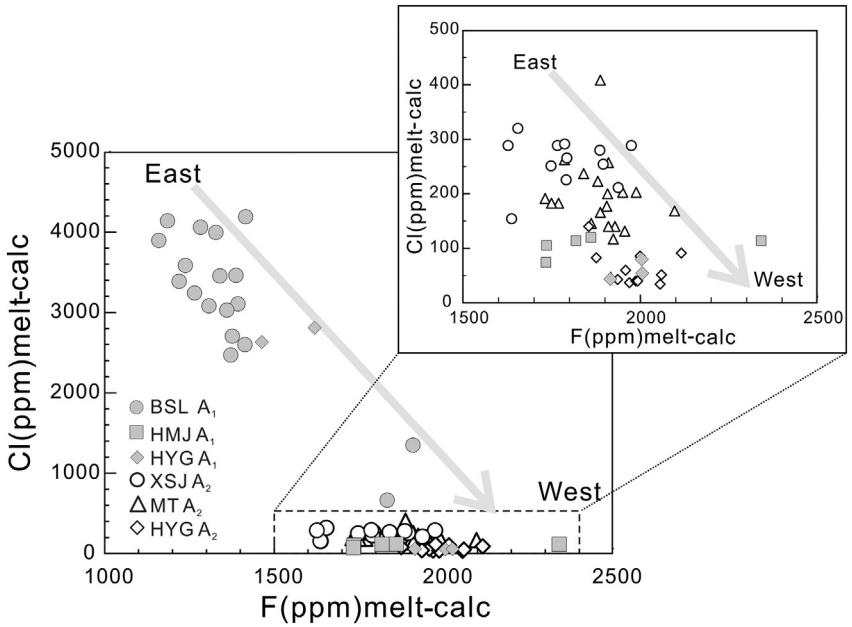

Fig. 6. Melt-F versus melt-Cl from the A-type granites in the LYRB.

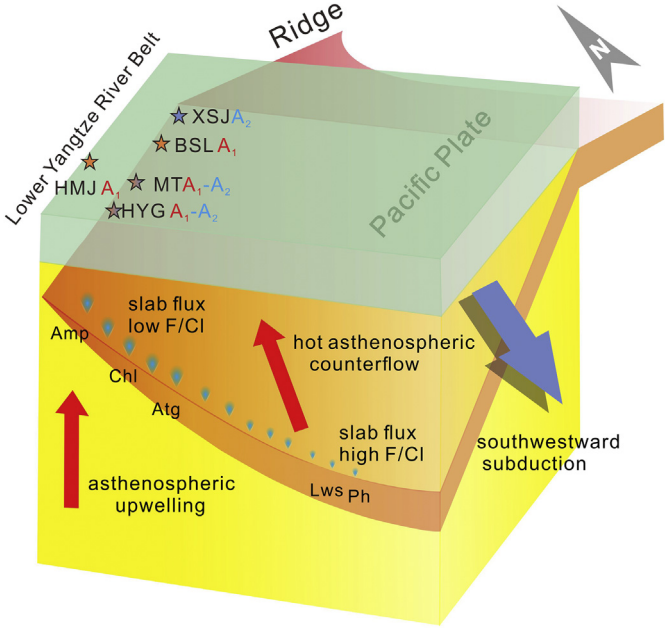

Fig. 8. Schematic illustration of a genetic model for formation of A-type granites in the LYRB. During the Early Cretaceous, the ridge between the Pacific plate and the Izanagi plate was subducted westwards to the LYRB and intersected with the subduction belt. The blue arrow represents that the Pacific plate subducted to the southwest. The red arrows indicates the asthenospheric upwelling and hot asthenospheric counterflow. The blue droplets show the upwelling of fluids derived from the decomposition of certain minerals during the process of the dehydration of the subducted slab. HMJ A_1-type granite was located directly above the ridge. HYG, MT, BSL and the XSJ A-type granites are situated away from the position of the ridge, and also gradually closer to the subduction zone. Amp = amphibole, Atg = antigorite, Chl = chlorite, Lws = lawsonite, Ph = phengite. (For interpretation of the references to color in this figure legend, the reader is referred to the web version of this article.)

subduction of the slab, the antigorite breaks down to secondary olivine, which has much lower REEs contents as well as a much lower LREE to HREE content. This will result in higher $(La/Yb)_N$ ratios in the fluids released at this stage (Debret et al., 2013), and might feasibly explain why several apatites from the HMJ A_1-type granite have the highest $(La/Yb)_N$ and $(Gd/Yb)_N$ ratios but less variation of $(La/Gd)_N$ (Fig. 4). Decomposition of phengite will produce fluids with flat MREE and HREE patterns (Schmidt et al., 2004). When residual garnet is present in the slab, the fluid may be enriched in LREE and have larger $(La/Gd)_N$, $(La/Yd)_N$ and lower $(Gd/Yb)_N$ ratios, because garnet prefers HREE, and to a lesser extent MREE, relative to LREE. This could explain the high F content (Fig. 2), high $(La/Gd)_N$, $(La/Yd)_N$ and low $(Gd/Yb)_N$ ratios (Fig. 4) in the source for the HYG A-type granite. Due to variations in phengite abundances in the subducting slab going in the direction opposite from that of the subduction zone, the source for the XSJ A_2-type granite appears to be related to metasomatism by slab dehydration fluids with varied $(La/Gd)_N$ and lower $(Gd/Yb)_N$ ratios (Fig. 4). Thus, the source of the A_2-type granite has a varied $(La/Gd)_N$ ratio, higher $(La/Yb)_N$ ratio and a negative correlation between the $(La/Gd)_N$ and $(Gd/Yb)_N$ ratios (Fig. 4).

In summary, Cl is released to fluids during the process of amphibolite facies grading into eclogite facies, in contrast to the F releasing under eclogite facies conditions due to the hot asthenospheric counterflow (Pagé et al., 2016). During early subduction, Cl is expelled at much shallower depths in the subduction zone through decomposition of amphibole, chlorite and/or serpentine (Figs. 7 and 8). As much as 75% of Cl in the subducted rocks and pore fluids may be released from the accretionary prism at slab depth < 15 km (Jarrard, 2003), metasomatising the overlying mantle wedge and further contributing to the formation of A_1-type granite. In contrast, F is mainly mineralogically retained and transported to the deep mantle (Fig. 8), leading to magmas derived from the deep mantle enriched in F in the A_2-type granite source rocks. Plutons containing both A_1- and A_2-type granites in the LYRB, such as HYG, are located at the transitional part of A_1- and A_2-type granites zones (Li et al., 2012a). This might be the result of heterogeneous source components influenced by different kinds of metasomatic fluids, other than late-stage magmatic evolutionary process, such as fractional crystallization.

5.3. Genetic model for A-type granites in the LYRB

Tectonic studies and plate reconstructions of eastern China and nearby regions during the Cretaceous all suggest that subduction of the Pacific and Izanagi plates was occurring in the coastal areas of eastern China (Li and Li, 2007; Ling et al., 2009; Maruyama et al., 1997; Sun et al., 2007b; Zhou and Li, 2000; Zhou et al., 2006; Fig. 1a). Previous studies have explained A-type granites as being the products of an extensional tectonic setting, caused by slab foundering (Li et al., 2013), or slab roll-back (Yang et al., 2016), or drift of subduction direction (Gu et al., 2017), or the presence of a slab window after ridge subduction (Li et al., 2011, 2012a; Ling et al., 2009). From the study of geochemical characteristics of apatites in the LYRB, it is apparent that chemical compositions of the apatites from A-type granites varied with location and relates to mantle metasomatism.

It is not possible to firmly establish the tectonic model responsible for the genesis of A-type granites based only on the geochemistry of apatites presented here. Determining a genetic model for these A-type granites requires further constraint by synthesizing data from previous studies on magmatic rocks in the LYRB.

During the Early Cretaceous (145–125 Ma), the Pacific Plate was drifting towards the southwest, while the Izanagi Plate was moving towards north-northwest at a higher speed (Maruyama et al., 1997; Sun et al., 2007b). Due to the different directions and rates of subduction, the ridge between these two plates moved westward during subduction and appears to have been subducted under eastern China and extending into the LYRB region (Ling et al., 2009, 2011; Sun et al., 2010). The early-stage subduction of the Pacific Plate produced 146–130 Ma adakites (younging from SW to NE), and Nb-rich basalts and related mineralization (e.g., Deng et al., 2016; Ling et al., 2009, 2011; Sun et al., 2010). During the later stage, the ~125 Ma A-type granites were emplaced (Li et al., 2012a). Zircon saturation thermometry of magmatic rocks in the LYRB indicates that the younger magmatic events are formed under the higher temperatures; the adakitic rocks show an average of 694 °C (Yan et al., 2015), and are contrasted to the A-type granites with an average of 797 °C (Gu et al., 2017; Zhao et al., 2016). The systematic changes in magma temperature suggest an increasing heat supply from the upwelling asthenosphere and an increasing intensity of extensional activity, which is also supported by numerical modeling results (Zhao et al., 2016). The early magmatic rocks were produced by both melting of the overlying mantle wedge and the subduction of oceanic crust associated with assimilation of enriched components in the lithospheric mantle and/or crustal materials (Li et al., 2010, 2013; Ling et al., 2009, 2011; Sun et al., 2010; Xie et al., 2011; Zhang et al., 2014). As the subduction continued, the spreading ridge opened and formed a slab window beneath eastern China, resulting in extensive upwelling of the asthenosphere. This provided sufficient heat to melt the enriched lithospheric mantle, which had been metasomatized by fluids and/or melts caused by the dehydration of the subducted slab, and played a key role in the generation of A-type granites. After the emplacement of A-type granites, the direction of Pacific Plate motion changed by ~80° from a roughly southward to a northwestward direction (Koppers et al., 2001; Sun et al., 2007b), resulting in a gradual closing of the slab window as the ridge ultimately disappeared (Zhao et al., 2016).

Previous studies suggest both A_1- and A_2-type granites, parallel to the LYRB, have diverse chemical compositions, but are related to distance from the ridge and subduction zone (Li et al., 2011, 2012a).

Above the ridge, the slab subducted at a shallow angle, initially giving off larger amounts of Cl relative to F from amphibole, serpentine and/or chlorite breakdown (Fig. 8). Under such circumstances, the A_1-type granites may form during an asthenosphere upwelling triggered by slab window opening and/or slab rollback. From the spreading ridge outwards to deeper down the slab, larger amounts of F relative to Cl were released due to phengite and/or lawsonite decomposition (Fig. 8). Consequently, A-type granites changed gradually from an A_1- to an A_2- chemical signature. A-type granites formed near the adakite belt therefore have both A_1- and A_2- characteristics, and the transition marks the extent of subduction-induced metasomatism (Li et al., 2012a; Fig. 1c). Such alternate distribution of A_1- to A_2-type granites (Fig. 1c), limited emplacement period (about 5 Ma) as well as their spatial association with the paleo-subduction belt (Figs. 1 and 8), favors an interpretation that ridge subduction together with roll-back controlled the formation of A-type granites in the LYRB.

6. Conclusions

(1) Apatites from A_1 and A_2 chemical subgroups have regularly variable geochemical compositions and volatile components, closely related to the spatial locations to the subduction zone/ridge. From the west to the east, the F concentrations decrease from 2.97 to 1.47 wt% and Cl concentrations increase from 0.01 to 1.47 wt%. Pulses of these halogen-rich fluids metasomatised the overlying mantle as a function of distance from the subduction zone/angle of subduction slab. The mantle wedge that was metasomatised close to the subduction zone/slab in shallow angle is more Cl-rich than mantle further away from the subduction zone/above the steeper slab, which is more F-rich.

(2) The geochemical information provided by apatite indicates that mantle metasomatism was critical to the petrogenesis of A-type granites. The compositional characteristics of the A_1- and A_2-type granites from the LYRB are controlled by source compositions, which are influenced by the fluids derived from breakdown of specific minerals during slab subduction. Cl-rich amphibole, chlorite and/or serpentine appear to have contributed to the formation of the A_1-type granite. Whereas F-rich phengite and/or lawsonite contributed more to the genesis of the A_2-type granite.

(3) The coexistence of A_1- and A_2-type granites in the same pluton can be produced by partial melting of heterogeneous source components affected by fluid metasomatism, rather than magmatic evolutionary process such as fractional crystallization.

Supplementary data to this article can be found online at https://doi.org/10.1016/j.lithos.2018.02.005.

Acknowledgements

This contribution was financially supported by the National Key R&D Program of China (2016YFC0600408), the Strategic Priority Research Program of the Chinese Academy of Sciences (No. XDB18000000), the Project funded by China Postdoctoral Science Foundation (Y701092001) and the National Natural Science Foundation of China (41473029). Professor Trevor Ireland is appreciated for constructive suggestions and help with English language. We thank Professor Xiaoyong Yang and Dr. Jianghong Deng for their assistance in fieldwork. This is a contribution of No. IS-0000 from GIG-CAS.

References

Bonin, B., 1988. Peralkaline granites in Corsica: some petrological and geochemical constraints. Rendiconti della Società Italiana di Mineralogia e Petrologia 43, 281–306.
Bonin, B., 2007. A-type granites and related rocks: evolution of a concept, problems and prospects. Lithos 97, 1–29.
Boyce, J.W., Hervig, R.L., 2009. Apatite as a monitor of late–stage magmatic processes at Volcán Irazú, Costa Rica. Contributions to Mineralogy and Petrology 157, 135–145.
Bruand, E., Fowler, M., Storey, C., Darling, J., 2017. Apatite trace element and isotope applications to petrogenesis and provenance. American Mineralogist 102, 75–84.
Churikova, T., Worner, G., Mironov, N., Kronz, A., 2007. Volatile (S, Cl and F) and fluid mobile trace element compositions in melt inclusions: implications for variable fluid sources across the Kamchatka arc. Contributions to Mineralogy and Petrology 154 (2), 217–239.
Clemens, J.D., Holloway, J.R., White, A.J.R., 1986. Origin of an A-type granite: experimental constraints. American Mineralogist 71, 317–324.
Collins, W.J., Beams, S.D., White, A.J.R., Chappell, B.W., 1982. Nature and origin of A-type granites with particular reference to southeastern Australia. Contributions to Mineralogy and Petrology 80, 189–200.
Creaser, R.A., Price, R.C., Wormald, R.J., 1991. A-type granites revisited: assessment of a residual-source model. Geology 19, 163–166.
Debret, B., Nicollet, C., Andreani, M., Schwartz, S., Godard, M., 2013. Three steps of serpentinization in an eclogitized oceanic serpentinization front (Lanzo Massif–Western Alps). Journal of Metamorphic Geology 31, 165–186.
Debret, B., Koga, K.T., Nicollet, C., Andreani, M., Schwartz, S., 2014. F, Cl and S input via serpentinite in subduction zones: implications for the nature of the fluid released at depth. Terra Nova 26, 96–101.
Deng, J.H., Yang, X.Y., Li, S., Gu, H.L., Mastoi, A.S., Sun, W.D., 2016. Partial melting of subducted paleo-Pacific plate during the early Cretaceous: Constraint from adakitic rocks in the Shaxi porphyry Cu–Au deposit, Lower Yangtze River Belt. Lithos 262, 651–667.
Deschamps, F., Godard, M., Guillot, S., Hattori, K., 2013. Geochemistry of subduction zone serpentinites: a review. Lithos 178, 96–127.
Dingwell, D.B., Hess, K.U., Romano, C., 1998. Extremely fluid behavior of hydrous peralkaline rhyolites. Earth and Planetary Science Letters 158, 31–38.
Doherty, A.L., Webster, J.D., Goldoff, B.A., Piccoli, P.M., 2014. Partitioning behavior of chlorine and fluorine in felsic melt–fluid(s)–apatite systems at 50MPa and 850–950 °C. Chemical Geology 384, 94–111.
Eby, G.N, 1990. The A-type granitiods - A review of their occurrence and chemical characteristics and speculations on their petrogenesis. Lithos 26, 115–134.
Eby, G.N., 1992. Chemical subdivision of the A-type granitoids: petrogenetic and tectonic implications. Geology 20, 641–644.
Fan, Y., Zhou, T.F., Yuan, F., Qian, C.C., Lu, S.M., Cooke, D., 2008. LA–ICP-MS zircon U–Pb ages of the A-type granites in the Lu-Zong (Lujiang–Zongyang) area and their geological significances. Acta Petrologica Sinica 24, 1715–1724 (in Chinese with English abstract).
Filiberto, J., Treiman, A.H., 2009. The effect of chlorine on the liquidus of basalt: First results and implications for basalt genesis on Mars and Earth. Chemical Geology 263, 60–68.
Frost, D.C., Frost, B.R., 2011. On ferroan (A-type) granitoids: their compositional variability and modes of origin. Jouranl of Petrology 52, 39–53.
Frost, B.R., Lindsley, D.H., 1991. Occurrence of iron-titanium oxides in igneous rocks: oxide minerals: petrologic and magmatic significance. Mineralogical Society of America, Reviews in Mineralogy and Geochemistry 25, 433–486.
Gu, H.L., Yang, X.Y., Deng, J.H., Duan, L.A., Liu, L., 2017. Geochemical and zircon U–Pb geochronological study of the Yangshan A-type granite: insights into the geological evolution in south Anhui, eastern Jiangnan Orogen. Lithos 284–285, 156–170.
Harlov, D.E., 2015. Apatite: a fingerprint for metasomatic processes. Elements 11, 171–176.
Huang, H.Q., Li, X.H., Li, W.X., Li, Z.X., 2011. Formation of high $\delta^{18}O$ fayalite-bearing A-type granite by high temperature melting of granulitic metasedimentary rocks, southern China. Geology 39, 903–906.
Hughes, J.M., Rakovan, J.F., 2015. Structurally robust, chemically diverse-apatite and apatite supergroup minerals. Elements 11, 165–170.
Jarrard, R.D., 2003. Subduction fluxes of water, carbon dioxide, chlorine, and potassium. Geochemistry, Geophysics, Geosystems 4 (5).
Kodolányi, J., Pettke, T., 2011. Loss of trace elements from serpentinites during fluidassisted transformation of chrysotile to antigorite — an example from Guatemala. Chemical Geology 284, 351–362.
Konzett, J., Frost, D.J., 2009. The high P–T stability of hydroxyl-apatite in natural and simplified MORB—an experimental study to 15 GPa with implications for transport and storage of phosphorus and halogens in subduction zones. Journal of Petrology 50, 2043–2062.
Koppers, A.A.P., Morgan, J.P., Morgan, J.W., Staudigel, H., 2001. Testing the fixed hotspot using $^{40}Ar/^{39}Ar$ age progressions along seamount trails. Earth and Planetary Science Letters 185, 237–252.
Kutoglu, A., 1974. Structure refinement of the apatite $Ca_5(VO_4)_3(OH)$. Neues Jahrbuch fuer Mineralogie, Monatshefte 5, 210–218.
Li, Z.X., Li, X.H., 2007. Formation of the 1300-km-wide intracontinental orogen and postorogenic magmatic province in Mesozoic South China: a flat-slab subduction model. Geology 35, 179–182.
Li, H., Zhang, H., Ling, M.X., Wang, F.Y., Ding, X., Zhou, J.B., Yang, X.Y., Tu, X.L., Sun, W.D., 2011. Geochemical and zircon U–Pb study of the Huangmeijian A-type granite: implications for geological evolution of the Lower Yangtze River belt. International Geology Review 53, 499–525.
Li, H., Ling, M.X., Li, C.Y., Zhang, H., Ding, X., Yang, X.Y., Fan, W.M., Li, Y.L., Sun, W.D., 2012a. A-type granite belts of two chemical subgroups in central eastern China: indication of ridge subduction. Lithos 150, 26–36.
Li, C.Y., Zhang, H., Wang, F.Y., Liu, J.Q., Sun, Y.L., Hao, X.L., Li, Y.L., Sun, W.D., 2012b. The formation of the Dabaoshan porphyry molybdenum deposit induced by slab rollback. Lithos 150, 101–110.
Li, H., Ling, M.X., Ding, X., Zhang, H., Li, C.Y., Liu, D.Y., Sun, W.D., 2014. The geochemical characteristics of Haiyang A-type granite complex in Shandong, eastern China. Lithos 200–201, 142–156.

Li, X.H., Li, W.X., Wang, X.C., Li, Q.L., Liu, Y., Tang, G.Q., Gao, Y.Y., Wu, F.Y, 2010. SIMS U-Pb zircon geochronology of porphyry Cu-Au-(Mo) deposits in the Yangtze River Metallogenic Belt, eastern China: magmatic response to early Cretaceous lithospheric extension. Lithos 119, 427–438.
Li, X.H., Li, Z.X., Zheng, X.L., Li, W.X., Wang, X.C., Gao, Y.Y., 2013. Revisiting the "C-type adakites" of the Lower Yangtze River Belt, central eastern China: In-situ zircon Hf-O isotope and geochemical constraints. Chemical Geology 345, 1–15.
Lin, J., Liu, Y.S., Yang, Y.H., Hu, Z.C., 2016. Calibration and correction of LA-ICP-MS and LA-MC-ICP-MS analyses for element contents and isotopic ratios. Solid Earth Sciences 1:5–27. https://doi.org/10.1016/j.sesci.2016.04.002.
Ling, M.X., Wang, F.Y., Ding, X., Hu, Y.H., Zhou, J.B., Zartman, R.E., Yang, X.Y., Sun, W.D., 2009. Cretaceous ridge subduction along the lower Yangtze River belt, eastern China. Economic Geology 104, 303–321.
Ling, M.X., Wang, F.Y., Ding, X., Zhou, J.B., Sun, W.D., 2011. Different origins of adakites from the Dabie Mountains and the Lower Yangtze River Belt, eastern China: geochemical constraints. International Geology Review 53, 727–740.
Liu, Y.S., Hu, Z.C., Gao, S., Gunther, D., Xu, J., Gao, C.G., Chen, H.H., 2008. In situ analysis of major and trace elements of anhydrous minerals by LA–ICP-MS without applying an internal standard. Chemical Geology 257, 34–43.
Loiselle, M.C., Wones, D.R., 1979. Characteristics and origin of anorogenic granites. Geological Society of America Abstracts with Programs 11 (468 pp.).
Lou, Y.E., Du, Y.S., 2006. Characteristics and zircon SHRIMP U–Pb ages of the Mesozoic intrusive rocks in Fanchang, Anhui Province. Geochimica 35, 333–345 (in Chinese with English abstract).
Maruyama, S., Isozaki, Y., Kimura, G., Terabayashi, M., 1997. Paleogeographic maps of the Japanese Islands: plate tectonic synthesis from 750 Ma to the present. Island Arc 6, 121–142.
Mathez, E.A., Webster, J.D., 2005. Partitioning behavior of chlorine and fluorine in the system apatite-silicate melt-fluid. Geochimica et Cosmochimica Acta 69, 1275–1286.
McDonough, W.F., Sun, S.S, 1995. The composition of the earth. Chemical Geology 120, 223–253.
Miles, A.J., Graham, C.M., Hawkesworth, C.J., Gillespie, M.R., Hinton, R.W., Bromiley, G.D., EMMAC, 2014. Apatite: a new redox proxy for silicic magmas? Geochimica et Cosmochimica Acta 132, 101–119.
Nash, W.P., 1984. Phosphate minerals in terrestrial igneous and metamorphic rocks. In: Nriaguand, J.O., Moore, B. (Eds.), Phosphate minerals. Springer-Verlag, Berlin, pp. 215–241.
Pagé, L., Hattori, K., de Hoog, J.C.M., Okay, A.I., 2016. Halogen (F, Cl, Br, I) behaviour in subducting slabs: a study of lawsonite blueschists in western Turkey. Earth and Planetary Science Letters 442, 133–142.
Parat, F., Holtz, F., Streck, M., 2011. Sulfur–bearing magmatic accessory minerals. Reviews in Mineralogy and Geochemistry 73, 285–314.
Patiño Douce, A.E., 1997. Generation of metaluminous A-type granites by low pressure melting of calc-alkaline granitoids. Geology 25, 743–746.
Piccoli, P., Candela, P., 1994. Apatite in felsic rocks; a model for the estimation of initial halogen concentrations in the Bishop Tuff (Long Valley) and Tuolumne Intrusive Suite (Sierra Nevada Batholith) magmas. American Journal of Science 294, 92–135.
Prowatke, S., Klemme, S., 2006. Trace element partitioning between apatite and silicate melts. Geochimica et Cosmochimica Acta 70, 4513–4527.
Rudnick, R.L., Gao, S., 2003. Composition of continental crust. In: Holland, HD, Turekian, KK (Eds.), The Crust Rudnick, RL The Crast. Treatise on Geochemistry 3. Elsevier, Oxford, pp. 1–64.
Scambelluri, M., Müntener, O., Ottolini, L., Pettke, T.T., Vannucci, R., 2004. The fate of B, Cl and Li in the subducted oceanic mantle and in the antigorite breakdown fluids. Earth and Planetary Science Letters 222, 217–234.
Schmidt, M.W., Poli, S., 2014. 4.19. Devolatilization during subduction. In: Rudnick, R.L. (Ed.), The Crust, Second edition In: Holland, H.D., Turekian, K.K. (Eds.), Treatise on Geochemistry. Elsevier-Pergamon, Oxford, pp. 669–701.
Schmidt, M.W., Vielzeuf, D., Auzanneau, E., 2004. Melting and dissolution of subducting crust at high pressures: the key role of white micas. Earth and Planetary Science Letters 228, 65–84.
Smythe, D.J., Brenan, J.M., 2016. Magmatic oxygen fugacity estimated using zircon-melt partitioning of cerium. Earth and Planetary Science Letters 453, 260–266.
Song, G.X., Qin, K.Z., Li, G.M., Evans, N., Li, X.H., 2014. Mesozoic magmatism and metallogeny in the Chizhou area, Middle-Lower Yangtze Valley, SE China: constrained by petrochemistry, geochemistry and geochronology. Journal of Asian Earth Sciences 91, 137–153.
Su, Y.P., Zheng, J.P., Griffin, W.L., Zhao, J.H., O'Reilly, S.Y., Tang, H.Y., Ping, X.Q., Xiong, Q., 2013. Petrogenesis and geochronology of Cretaceous adakitic, I-and A-type granitoids in the NE Yangtze block: constraints on the eastern subsurface boundary between the North and South China blocks. Lithos 175–176, 333–350.
Sun, S.S., McDonough, W.F., 1989. Chemical and isotopic systematics of oceanic basalts: implications formantle composition andprocesses. In: Saunders, A.D., Norry, M.J. (Eds.), Magmatism in the Ocean Basalts. Geological Society Special Publication, pp. 313–345.
Sun, W.D., Binns, R.A., Fan, A.C., Kamenetsky, S., Wysoczanski, R., Wei, G.J., Hu, Y.H., Arculus, R.J., 2007a. Chlorine in submarine volcanic glasses from the eastern manus basin. Geochimica et Cosmochimica Acta 71, 1542–1552.
Sun, W.D., Ding, X., Hu, Y.H., Li, X.H., 2007b. The golden transformation of the Cretaceous plate subduction in the west Pacific. Earth and Planetary Science Letters 262, 533–542.
Sun, W.D., Ling, M.X., Yang, X.Y., Fan, W.M., Ding, X., Liang, H., 2010. Ridge subduction and porphyry copper–gold mineralization: an overview. Science in China Series D: Earth Sciences 53, 475–484.
Watson, E.B., Harrison, T.M., 2005. Zircon thermometer reveals minimum melting conditions on earliest Earth. Science 308, 841–844.
Webster, J.D., Piccoli, P.M., 2015. Magmatic apatite: a powerful, yet deceptive, mineral. Elements 11, 177–182.
Webster, J.D., Tappen, C.M., Mandeville, C.W., 2009. Partitioning behavior of chlorine and fluorine in the system apatite–melt–fluid. II: felsic silicate systems at 200 MPa. Geochimica et Cosmochimica Acta 73, 559–581.
Whalen, J.B., Currie, K.L., Chappell, B.W., 1987. A-type granites: geochemical characteristics, discrimination and petrogenesis. Contributions to Mineralogy and Petrology 95, 407–419.
Wilson, A., Sudarsanan, K., Young, R., 1977. The structures of some cadmium "apatites" $Cd_5(MO_4)_3X$. II. The distributions of the halogen atoms in $Cd_5(VO_4)_3I$, $Cd_5(PO_4)_3Br$, $Cd_5(AsO_4)_3Br$, $Cd_5(VO_4)_3Br$ and $Cd_5(PO_4)_3Cl$. Acta Crystallographica. Section B: Structural Crystallography & Crystal Chemistry 33, 3142–3154.
Wong, J., Sun, M., Xing, G.F., Li, X.H., Zhao, G.C., Wong, K., Yuan, C., Xia, X.P., Li, L.M., Wu, F.Y., 2009. Geochemical and zircon U–Pb and Hf isotopic study of the Baijuhuajian metaluminous A-type granite: extension at 125–100 Ma and its tectonic significance for South China. Lithos 112, 289–305.
Wu, C.L., Zhou, X.R., 1998. A-type granites in Maotan, Anhui. Acta Geologica Sinica 72, 237–248 (in Chinese with English abstract).
Xie, G.Q., Mao, J.W., Li, X.W., Duan, C., Yao, L., 2011. Late Mesozoic bimodal volcanic rocks in the Jinniu basin, Middle-Lower Yangtze River Belt (YRB), East China: age, petrogenesis and tectonic implications. Lithos 127, 144–164.
Xing, F.M., Xu, X., 1994. Two A-type granite belts from Anhui. Acta Petrologica Sinica 10, 257–269 (in Chinese with English abstract).
Xiong, X.L., Adam, J., Green, T.H., 2005. Rutile stability and rutile/melt HFSE partitioning during partial melting of hydrous basalt: implications for TTG genesis. Chemical Geology 218, 339–359.
Xiong, X.L., Keppler, H., Audetat, A., Gudfinnsson, G., Sun, W.D., Song, M.S., Xiao, W.S., Yuan, L., 2009. Experimental constraints on rutile saturation during partial melting of metabasalt at the amphibolite to eclogite transition, with applications to TTG genesis. American Mineralogist 94, 1175–1186.
Xue, H.M., Wang, Y., Ma, F., Wang, C., Wang, D., Zuo, Y.L., 2009. The Huangshan A-type granites with tetrad REE: constraints on Mesozoic lithospheric thinning of the southeastern Yangtze craton? Acta Geologica Sinica 83, 247–259 (in Chinese with English abstract).
Yan, J., Liu, J.M., Li, Q.Z., Xing, G.F., Liu, X.Q., Xie, J.C., Chu, X.Q., Chen, Z.H., 2015. In situ zircon Hf–O isotopic analyses of late Mesozoic magmatic rocks in the Lower Yangtze River Belt, central eastern China: implications for petrogenesis and geodynamic evolution. Lithos 227, 57–76.
Yang, J.H., Wu, F.Y., Chung, S.L., Wilde, S.A., Chu, M.F., 2006. A hybrid origin for the Qianshan A-type granite, northeast China: geochemical and Sr–Nd–Hf isotopic evidence. Lithos 89, 89–106.
Yang, W., Zhang, H.F., 2012. Zircon geochronology and Hf isotopic composition of Mesozoic magmatic rocks from Chizhou, the Lower Yangtze Region: constraints on their relationship with Cu–Au mineralization. Lithos 150, 37–48.
Yang, Y.Z., Wang, Y., Ye, R.S., Li, S.Q., He, J.F., Siebel, W., Chen, F.K., 2016. Petrology and geochemistry of Early Cretaceous A-type granitoids and late Mesozoic mafic dikes and their relationship to adakitic intrusions in the lower Yangtze River belt, Southeast China. International Geology Review 1, 62–79.
Zhang, B.D., Zhang, F.S., Ni, Q.S., Chen, P.R., Zhai, J.P., Shen, W.Z., 1988. Geology geochemistry and genisis discution of quartz syenite in Anlu belt. Acta Petrologica Sinica 3, 1–12 (in Chinese with English abstract).
Zhang, S., Zhang, Z.C., Ai, Y., Yuan, W.M., Ma, L.T., 2009. The petrology, mineralogy and geochemistry study of the Huangshan granite intrusion in Anhui Province. Acta Petrologica Sinica 25, 25–38 (in Chinese with English abstract).
Zhang, C., Holtz, F., Ma, C., Wolff, P.E., Li, X., 2012. Tracing the evolution and distribution of F and Cl in plutonic systems from volatile-bearing minerals: a case study from the Liujiawa pluton (Dabie orogen, China). Contributions to Mineralogy and Petrology 164, 859–879.
Zhang, Z.Y., Du, Y.S., Teng, C.Y., Zhang, J., Pang, Z.S., 2014. Petrogenesis, geochronology, and tectonic significance of granitoids in the Tongshan intrusion, Anhui Province, Middle–Lower Yangtze River Valley, eastern China. Journal of Asian Earth Sciences 79, 792–809.
Zhao, L., Guo, F., Fan, W.M., Zhang, Q.W., Wu, Y.M., Li, J.Y., Yan, W., 2016. Early Cretaceous potassic volcanic rocks in the Jiangnan Orogenic Belt, East China: crustal melting in response to subduction of the Pacific–Izanagi ridge? Chemical Geology 437, 30–43.
Zheng, Y.F., Fu, B., Gong, B., 1995. The thermal history of the Huangmeijian intrusion in Anhui and its relation to mineralization: isotopic evidence. Acta Geologica Sinica 69, 337–348 (in Chinese with English abstract).
Zhou, X.M., Li, W.X., 2000. Origin of Late Mesozoic igneous rocks in Southeastern China: implications for lithosphere subduction and underplating of mafic magmas. Tectonophysics 326, 269–287.
Zhou, X.M., Sun, T., Shen, W.Z., Shu, L.S., Niu, Y.L., 2006. Petrogenesis of Mesozoic granitoids and volcanic rocks in South China: a response to tectonic evolution. Episodes 29, 26–33.